Available online at www.sciencedirect.com
ScienceDirect
Journal of Electron Spectroscopy and Related Phenomena 156–158 (2007) 68–72
JOURNAL OF ELECTRON SPECTROSCOPY and Related Phenomena
www.elsevier.com/locate/elspec

Electron–ion multiple coincidence spectroscopy for small molecules and clusters

Norio Saito [a,*], Xiao Jing Liu [b], Yuichiro Morishita [a], Isao H. Suzuki [a,c], Kiyoshi Ueda [b]

[a] National Institute of Advanced Industrial Science and Technology (AIST), NMIJ, Tsukuba 305-8568, Japan
[b] Institute of Multidisciplinary Research for Advanced Materials, Tohoku University, Sendai 980-8577, Japan
[c] Photon Factory, Institute of Material Structure Science, Oho 1-1, Tsukuba 980-0801, Japan

Available online 1 December 2006

Abstract

We have developed an electron–ion multiple coincidence technique at BL27SU at SPring-8 in Japan, which consists of electron and ion time-of-flight analyzers with multi-hit two-dimensional position sensitive detectors and a supersonic jet from a cooled nozzle. Recent studies on the electron–ion multiple coincidence experiments using this apparatus are reviewed in this paper. We discuss N 1s photoelectron angular distributions in the molecular frame for NO using a new projection analysis method. As an example of de-excitation processes, we have observed interatomic Coulombic decay (ICD) from an Auger-final dicationic state with 3s and 3p holes in the Ar trimer. This ICD process is unambiguously identified by the electron–ion–ion–ion coincidence technique in which the kinetic energy of the ICD electron and the kinetic energy release in the three Ar^+ fragmentation are measured in coincidence.

PACS: 36.40.Mr; 33.60.Fy; 33.80.Eh

Keywords: Multiple coincidence momentum imaging; Photoelectron angular distribution; Fixed-in-space molecule; NO; Ar trimer; Interatomic Coulombic decay

1. Introduction

An electron–ion multiple coincidence momentum imaging spectroscopy has progressed greatly in these years and can now yield a great deal of information on dynamics of photoexcitation and photoionization. This system generally consists of electron and ion time-of-flight analyzers with multi-hit two-dimensional position sensitive detectors and a supersonic jet. Using this technique, one can extract momentum correlations between all electrons and ions detected. Initially this technique was developed for detection of the momentum of a recoil ion from the double photoionization of He [1]. This technique is nowadays known as COLTRIMS. They measured the vector correlations between one of photoelectrons and the recoil doubly ionized ion. Immediately this technique was applied to studies of diatomic molecules, which showed 1s photoelectron angular distributions in the molecular frame (MFPAD) from N_2 and CO [2–4]. It took very short time to realize a utilization of this technique to larger molecules such as CO_2 and HCCH [5–7]. The apparatus has been developed for observation of MFPADs in higher energy resolution which enable us to find vibrational structure [8,9]. On the other hand, this technique was applied to probe of nuclear motion and symmetry on photoionization and photoexcitation of molecules. The nuclear motions of core-excited CO_2, BF_3 and HCCH molecules were probed using this technique [10–14]. It was found that the CO_2 molecules in the C/O $1s^{-1}$ π^* A_1 and B_1 Renner–Teller states are bent in the A_1 state and linear in the B_1 state [10,11]. Symmetry-resolved photoionization of CO_2 and NO_2 molecules [15–17] were also investigated using this technique. Recently this technique was applied to clusters [18–21]. Jahnke et al. [19] reported a clear experimental evidence for interatomic Coulombic decay (ICD) [22] in 2s ionized Ne dimers by identifying this process unambiguously using electron–ion–ion coincidence spectroscopy in which the kinetic energy of the ICD electron and the total kinetic energy release (KER) between the two Ne^+ ions were measured in coincidence. Morishita et al. [20] reported a clear experimental evidence for ICD in Ar dimers after the normal

* Corresponding author.
E-mail address: norio.saito@aist.go.jp (N. Saito).

0368-2048/$ – see front matter © 2006 Elsevier B.V. All rights reserved.
doi:10.1016/j.elspec.2006.11.048

atomic Auger decay, by employing the electron–ion–ion coincidence spectroscopy. As described above, electron–ion multiple coincidence momentum imaging spectroscopy is very powerful in probing photoionization or photoexcitation dynamics of atoms, molecules and clusters. To demonstrate the power of the electron–ion multiple coincidence spectroscopy, we review two case studies, MFPAD measurements for the N 1s photoionization of NO [23] and two-step interatomic decay in Ar_3 [24], among our recent works.

2. Experimental

The experiment was carried out on the c branch of the soft X-ray photochemistry beam line 27SU [25,26] at SPring-8. The storage ring was operated in the 73 single-bunches +10/84 filling mode, which provides a single-bunch separation of 57.0 ns. The coincidence measurements described below were performed with the *E* vector orientated vertically. The photon beam was focused to a size less than 0.2 mm in height and 0.5 mm in width at the point of crossing with the molecular beam. The present electron–ion multiple coincidence momentum imaging is based on recording the electron and ion times-of-flight (TOFs) with multi-hit two-dimensional position sensitive detectors [5,10,15,27–29]. The two TOF spectrometers are placed face to face, and the TOF spectrometer axis is horizontal and perpendicular to both the photon beam and the molecular beam. The lengths of the acceleration region and the drift region of the electron spectrometer are 33.7 and 67.4 mm, respectively. For the ion spectrometer, there are two acceleration regions and no drift region. The length of the first acceleration region is 16.5 mm and that of the second one is 82.5 mm. The TOF spectrometer for the electron is equipped with a hexagonal multi-hit position-sensitive delay-line detector of effective diameter of 120 mm, while that for the ion is of effective diameter 80 mm. The TOFs of the electrons and ions were recorded with respect to the bunch marker of the synchrotron radiation source using ultra-fast multi-hit time-to-digital converters (TDCs). These TDCs have a timing resolution of about 120 ps, a multi-hit capability of up to six events, and a time span of 40 μs [30]. Appropriate gates select only those electron signals synchronized with the single bunches, and we record only events in which at least one ion (or two ions) and one electron are detected in coincidence. Knowledge of position and arrival time on the particle detectors (x, y, t), allows us to extract information about the linear momentum (p_x, p_y, p_z) for each particle.

In the experiment for NO, N 1s MFPADs was measured using electron–ion–ion coincidence mode at a photon energy of 412 eV, which is 1.6 eV above the N $1s^{-1}$ $^3\Pi$ ionization threshold. The photon energy bandwidth was 80 meV. The NO molecular beam was produced at a stagnation pressure of 1.0 bar through a pinhole of 30 μm diameter and 0.25 mm thickness. The static extraction field was set to 0.5 V/mm. The static field of the second acceleration region for the ions was set to 30 V/mm. A uniform magnetic field of 1.5 G was superimposed to the spectrometer by a set of Helmholtz coils outside the vacuum chamber. In the experiment for Ar trimer, Ar trimers were produced by expanding Ar gas at a stagnation pressure of 1.2 bar with a gas nozzle cooled to a temperature of about 125 K. The cluster beam was directed vertically and the trimer fraction in the cluster beam was estimated to be at least 0.1%. The electron–ion–ion–ion coincidence measurements were performed for Ar_3 at a photon energy of 262 eV, i.e. 13.4 and 11.3 eV above the atomic Ar $2p^{-1}$ $^2P_{3/2}$ and $2p^{-1}$ $^2P_{1/2}$ ionization thresholds [31]. The photon bandwidth was ~30 meV. The static extraction field was set to 1.42 V/mm and a uniform magnetic field of 5.8 G was superimposed.

3. Molecular frame photoelectron angular distributions of NO

We have investigated molecular frame photoelectron angular distributions (MFPADs) of NO, which will be described else-

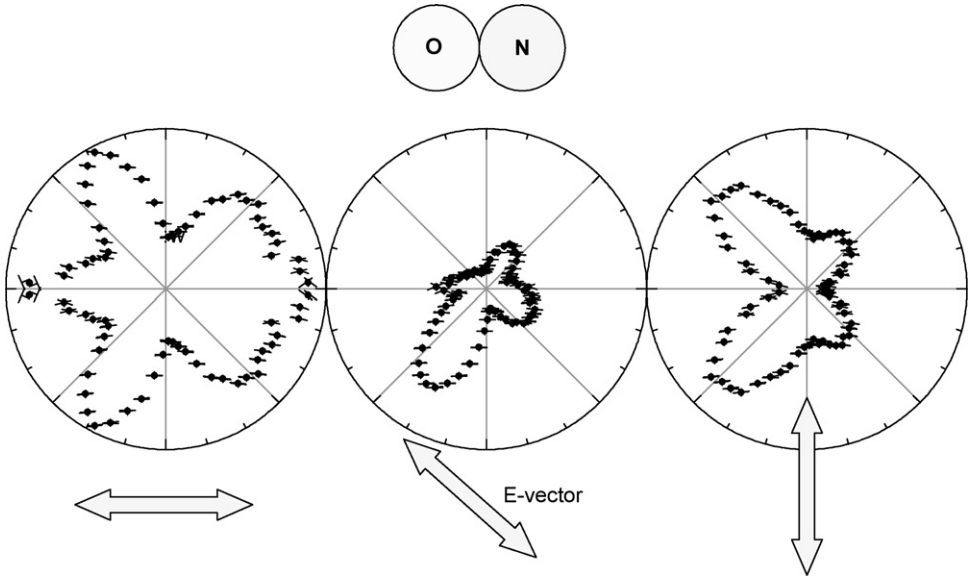

Fig. 1. N 1s MFPADs on the plane with the molecular axis and *E* vector. The molecular axis is horizontal and the *E* vector is 0°, 45°, and 90° with respect to the molecular axis.

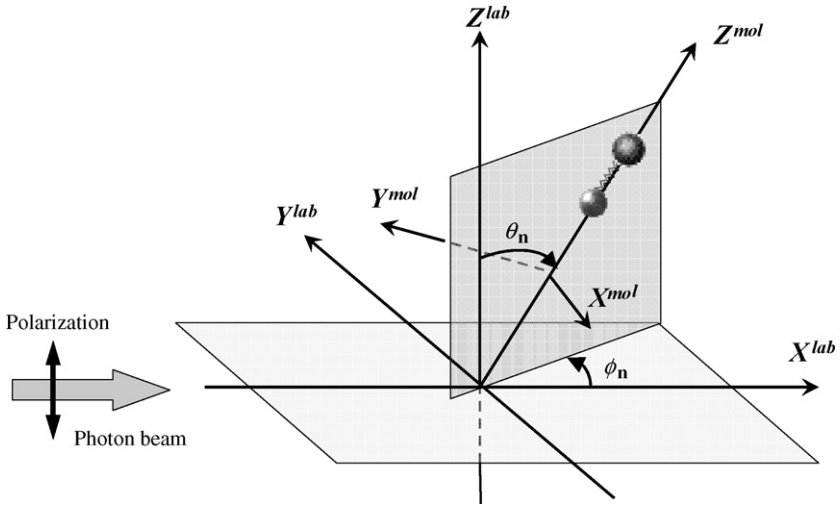

Fig. 2. Orientation of the molecular frame relative to the laboratory frame. Note that for the case of linear molecules considered here we have taken the X^{mol} axis to lie in the plane defined by the Z^{mol} and Z^{lab} axes.

where. Here we present only the result at a photon energy of 412 eV [23], which is 1.6 eV above the N $1s^{-1}$ $^3\Pi$ ionization threshold. Fig. 1 shows the N 1s MFPADs for $^3\Pi$ of NO. The MFPADs are illustrated for the angles of the electric vector of 0°, 45°, and 90° with respect to the molecular axis. The electron emission is within the plane defined by the molecular axis and the electric vector of the incident radiation. There is no MFPADs measured at corresponding photon energy in the previous work but Hosaka et al. [32] measured the MFPADs at a photon energy of 413.5 eV, in which the electron energy for $^1\Pi$ was 1.7 eV. This electron energy is close to the present $^3\Pi$ electron energy of 1.6 eV. The structure of the MFPADs is in principle close each other. They provided the MFPADs only for the case that the molecular axis is parallel to the polarization direction of photon.

We have measured the full 4π angular distributions of the photoelectron and ion directions. MFPADs in Fig. 1 are illustrated for only three angles of molecular axis directions and for electron emission within a plane defined by the molecular axis and the electric vector and thus only a small part of the information about MFPADs is reflected. Here we apply a new projection method to our data and extract full functional information about MFPAD [23]. The projection method is briefly explained as follows. In the dipole approximation with linearly polarized light, the light can be characterized by a polarization direction. In Fig. 2 this is given by the Z^{lab} axes. Then for linear molecules the MFPAD will only depend on three angles, θ and ϕ which give the direction of emission of the photoelectron in the molecular frame, and θ_n which gives the polar angle between the molecular axis and the photon polarization direction. The MFPAD does not depend on ϕ_n which gives the azimuthal angle of the molecular axis. The Z^{mol} axis was set to the molecular axis. The X^{mol} axis was set to be located in the plane defined by the Z^{mol} and Z^{lab} axes. In the case of the linear molecule, the MFPAD can be written using the associated Legendre polynomials (P_J^N) as [33]:

$$I(\theta, \phi, \theta_n) = F_{00}(\theta) + F_{20}(\theta)P_2^0(\cos\theta_n) + F_{21}(\theta)P_2^1(\cos\theta_n)\cos\phi + F_{22}(\theta)P_2^2(\cos\theta_n)\cos 2\phi. \quad (1)$$

Our projection method is to use the fact the expansion in Eq. (1) is in terms of orthogonal polynomials of θ_n and ϕ such that the $F_{JN}(\theta)$ can be obtained as

$$F_{JN}(\theta) = \frac{(2J+1)(J-N)!}{2\pi(1+\delta_{N,0})(J+N)!} \int_0^{\pi} \sin\theta_n \, \mathrm{d}\theta_n \int_0^{2\pi} \mathrm{d}\phi I(\theta, \phi, \theta_n) P_J^N(\cos\theta_n)\cos(N\phi). \quad (2)$$

This approach has been used here to extract the MFPAD for N 1s photoionization of NO.

In Fig. 3 we present the experimental F_{JN} functions determined from usage of the projection method given in Eq. (2). The $\theta = 0°$ direction corresponds to the direction that the N^+ atom was emitted and $\theta = 180°$ corresponds to the direction of emission of the O^+ atom. The experimental cross-sections are relative and thus the F_{JN} functions are normalized to dimensionless $\bar{F}_{JN}$ functions where

$$\int_0^{\pi} \sin\theta \, \mathrm{d}\theta \int_0^{2\pi} \mathrm{d}\phi \bar{F}_{00}(\theta) = 4\pi. \quad (3)$$

Using the obtained $\bar{F}_{JN}$ functions, we can reconstruct MFPADs for any angles between the molecular axis and the polarization vector. MFPADs in Fig. 1 were in fact the ones reconstructed from $\bar{F}_{JN}$ functions in Fig. 3.

4. Sequential interatomic Coulombic decay in argon trimers

In ICD, an atom with an innervalence vacancy can transfer its energy to a neighboring species which subsequently releases its energy by emitting an electron from its outervalence orbital [22,34]. Though ICD can take place without having an overlap of the orbitals, via a transfer of a virtual photon. Averbukh et al. showed that even in loosely bound van der Waals clusters, the orbital overlap is a crucial factor [35]. The ICD can be very fast depending on the environments [36]. ICD can emerge also after atomic Auger decay in clusters [37]. We have investigated

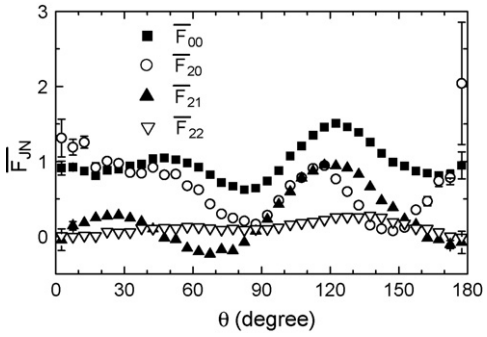

Fig. 3. F_{JN} functions for photoionization of NO leading to the N $1s^{-1}$ $^3\Pi$ state of NO^+ at a photon energy of 412 eV. The error bars are shown in case that the size of error is larger than the size of a data mark.

the sequential decay from the 2p inner-shell hole state in the Ar trimer. We focus on the production of the three Ar^+ ions from Ar_3. This process is of particular interest because it implies that two sequential *interatomic* decay should be involved. The triple ionization thresholds of Ar atom and Ar_3 cluster are 84.27 and ~57 eV, respectively.

Fig. 4 shows an Ar cluster ion–ion coincidence spectrum. The x and y coordinates correspond to the TOFs of the first and the second ions of the coincidence pair. Ar^{2+} and Ar^+ ions with zero momentum are located at TOFs of 3.25 and 4.61 μs, illustrated by dashed (Ar^{2+}) and dotted (Ar^+) lines in the figure. One can see clearly the lines corresponding to fragmentation into Ar^+–Ar^+ and Ar^{2+}–Ar^+. The broad cloud between the lines of Ar^+–Ar^+ and Ar^{2+}–Ar^+ is the coincidence signals from Ar^+–Ar^+–Ar^+.

Our coincidence measurement for one electron and three ions provides the electron kinetic energy together with the KER among the three ions for each event. The relationship of the electron energy and the KER in the fragmentation into

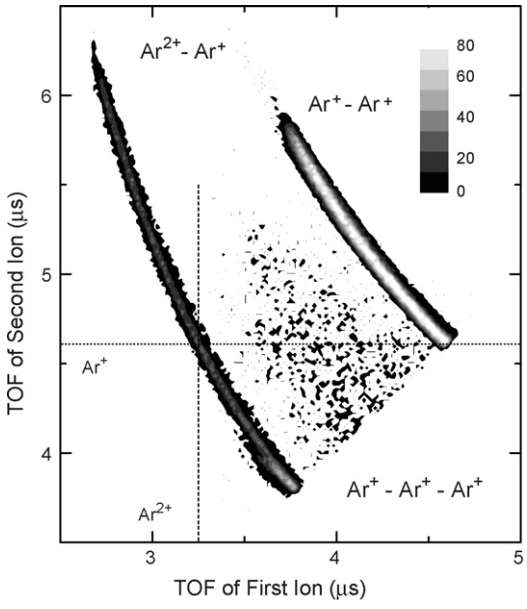

Fig. 4. Ar cluster ion–ion coincidence TOF spectrum. The dashed line shows the time-of-flight for zero-momentum Ar^{2+} ions, the dotted line for zero-momentum Ar^+ ions.

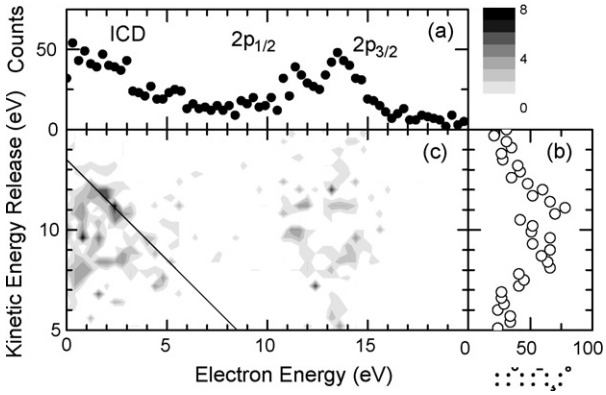

Fig. 5. (a) Energy distribution of the electrons ejected from the Ar trimers. (b) The total kinetic energy release (KER) among the three Ar^+ ions of the Ar_3 fragmentation. (c) Relationship between the electron energy and the KER.

Ar^+–Ar^+–Ar^+ is shown in Fig. 5. Fig. 5(a) shows the electron energy distribution in coincidence with the fragmentation into Ar^+–Ar^+–Ar^+. The two peaks located at 11.3 and 13.5 eV correspond to photoelectrons from the Ar $2p_{1/2}$ and $2p_{3/2}$ inner-shells. These energies coincide with the atomic energies within an experimental uncertainty of <0.5 eV, as in the case of Ar_2 [18,20]. The electron emission below ~5 eV appreciably corresponds to the ICD electrons, as we will discuss below. Fig. 5(b) shows the distribution of the KER among the three Ar^+ from the Ar_3. There seem to be two peaks at about 11 and 9 eV. If one assumes pure Coulomb explosion, the energies 11 and 9 eV correspond to the internuclear distances of 3.9 and 4.8 Å, respectively. These values are to be compared with the bond length of the neutral Ar_3 3.8 Å[38]. The higher KER peak corresponding to the 3.9 Å distance suggests that the charge separation takes place instantaneously after inner-shell ionization. The larger internuclear distance 4.8 Å than the equivalent bond length 3.8 Å, on the other hand, may imply that the charge separation takes place slightly later after nuclear motion by nearly 1 Å.

Fig. 5(c) shows the correlation between the electron kinetic energy and the KER. The islands in the right hand side are attributed to photoelectrons as described above. On the left hand side, one can see clearly one island that tilts with a slope of −1. The straight line with the slope of −1 indicates that the sum of the kinetic energy of the ICD electron and the KER among the three Ar^+s is 13.6 eV. Thus, we can identify this island as corresponding to the ICD process following the Auger decay. The straight line with the slope of −1 suggests that the three Ar^+s are not produced through a process of simultaneous two electron emission such as double Auger decay but they are produced through a sequential process from an Auger final state of Ar_3.

The final Ar^+ ions are in the $3p^{-1}$ ground state, whose energy relative to the neutral ground state is 15.75 eV. Thus the energy of the first-step Auger final dicationic state identified above can be estimated to be $15.75 \times 3 + 13.6 = 60.85 \pm 0.50$ eV. This energy coincides with the energy 61.23 eV of the atomic Ar dicationic states $3s^{-1}3p^{-1}$ ^{1}P [39]. Thus the final state of the first-step Auger decay may be considered to be the $Ar^{2+}(3s^{-1}3p^{-1}$ ^{1}P)–Ar–Ar one-site two-hole states. If these Auger final states

were a pure one-site two-hole state, however, the second-step Auger decay (ICD) would not lead to the three-site hole states $Ar^+(3p^{-1})$–$Ar^+(3p^{-1})$–$Ar^+(3p^{-1})$. Therefore we expect that $Ar^{2+}(3s^{-1}3p^{-1}\ ^1P)$–Ar–Ar one-site two-hole states couple with the two-site satellite states such as $Ar^+(3p^{-2}n\ell)$–$Ar^+(3p^{-1})$–Ar. The first-step Auger decay leads to these coupled states due to the $Ar^{2+}(3s^{-1}3p^{-1}\ ^1P)$–Ar–Ar one-site two-hole character, whereas the second-step ICD leads to the final three-site state $Ar^+(3p^{-1})$–$Ar^+(3p^{-1})$–$Ar^+(3p^{-1})$ due to the $Ar^+(3p^{-2}n\ell)$–$Ar^+(3p^{-1})$–Ar, in which the $n\ell$ electron fills the 3p hole in the same site and one 3p electron is emitted as an ICD electron from the third Ar site.

5. Conclusion

Recent studies on the electron–ion multiple coincidence experiments are reviewed. We have measured N 1s MFPADs for NO at the photon energy of 412 eV. The four F_{JN} functions has been obtained for the N 1s photoionization of NO using a new projection method. We have also investigated sequential interatomic Coulombic decay in Ar_3. The first-step Auger decay of the 2p hole state in Ar_3 leads to the one-site two-hole states $Ar^{2+}(3s^{-1}3p^{-1})$–Ar–Ar that couples to the two-site satellite states $Ar^+(3p^{-2}n\ell)$–$Ar^+(3p^{-1})$–Ar. These states are subject to ICD to the states $Ar^+(3p^{-1})$–$Ar^+(3p^{-1})$–$Ar^+(3p^{-1})$ via the two-site satellite character, where the $n\ell$ electron fills the 3p hole in the same Ar site and one of the 3p electrons in the third Ar site is emitted as a slow ICD electron. This ICD process is unambiguously identified by the electron–ion–ion–ion coincidence technique in which the kinetic energy of the ICD electron and the kinetic energy release in the three Ar^+ fragmentation are measured in coincidence.

Acknowledgments

The experiments were performed at SPring-8 with the approval of the program review committee (2006A1216-NSb-np, 2006A1757-NSb-np, 2005A0022-NSb-np, and 2005A2367-CSb-np). The work was partly supported by Grants-in-Aid for Scientific Researches from the Japan Society for Promotion of Science and by the Budget for Nuclear Research from Ministry of Education, Culture, Sports, Science and Technology, based on screening and counseling by the Atomic Energy Commission. The authors are grateful to G. Prümper, H. Fukuzawa, R. Richter, Y. Tamenori, and J.R. Harries for their invaluable contributions to the experimental parts, and to R.R. Luccese, R. Montuoro, A.N. Grum-Grzhimailo, S. Stoychev, A. Kuleff, and L.S. Cederbaum for discussion and theoretical supports.

References

[1] R. Dörner, et al., Phys. Rev. A 57 (1998) 1074.
[2] A. Landers, et al., Phys. Rev. Lett. 87 (2001) 013002.
[3] Th. Weber, et al., J. Phys. B: At. Mol. Opt. Phys. 34 (2001) 3669.
[4] T. Jahnke, et al., Phys. Rev. Lett. 88 (2002) 073002.
[5] N. Saito, et al., J. Phys. B: At. Mol. Opt. Phys. 36 (2003) L25.
[6] N. Saito, et al., J. Phys. B: At. Mol. Opt. Phys. 38 (2005) L277.
[7] T. Osipov, et al., Phys. Rev. Lett. 90 (2003) 233002.
[8] T. Jahnke, et al., Phys. Rev. Lett. 93 (2004) 083002.
[9] N. Saito, et al., Phys. Rev. A 72 (2005) 042717.
[10] Y. Muramatsu, et al., Phys. Rev. Lett. 88 (2002) 133002.
[11] N. Saito, et al., J. Electron Spectrosc. Relat. Phenom. 141 (2004) 133.
[12] K. Ueda, et al., Chem. Phys. 289 (2003) 135.
[13] A. De Fanis, et al., Phys. Rev. A 69 (2004) 022506.
[14] N. Saito, et al., Chem. Phys. Lett. 393 (2004) 295.
[15] A. De Fanis, et al., Phys. Rev. Lett. 89 (2002) 023006.
[16] A. De Fanis, et al., J. Electron Spectrosc. Relat. Phenom. 137–140 (2004) 265.
[17] N. Saito, et al., Phys. Rev. A 70 (2004) 062724.
[18] A. De Fanis, et al., J. Phys. B: At. Mol. Opt. Phys. 37 (2004) L235.
[19] T. Jahnke, et al., Phys. Rev. Lett. 93 (2006) 163401.
[20] Y. Morishita, et al., Phys. Rev. Lett. 96 (2006) 243402.
[21] K. Ueda, X.-J. Liu, H. Fukuzawa, G. Prümper, Y. Morishita, N. Saito, J. Electron Spectrosc. Relat. Phenom. 155 (2007) 113.
[22] L.S. Cederbaum, J. Zobeley, F. Tarantelli, Phys. Rev. Lett. 79 (1997) 4778.
[23] R.R. Lucchese, R. Montuoro, A.N. Grum-Grzhimairo, X.-J. Liu, G. Pruemper, Y. Morishita, N. Saito, K. Ueda, J. Electron Spectrosc. Relat. Phenom. 155 (2007) 95.
[24] X-J. Liu, N. Saito, H. Fukuzawa, Y. Morishita, S. Stoychev, A. Kuleff, I.H. Suzuki, Y. Tamenori, R. Richter, G. Prümper, K. Ueda, J. Phys. B: At. Mol. Opt. Phys. 40 (2007) F1.
[25] H. Ohashi, et al., Nucl. Instrum. Meth. A 467–468 (2001) 529.
[26] K. Ueda, J. Phys. B: At. Mol. Opt. Phys. 36 (2003) R1.
[27] Y. Morishita, et al., Radiat. Phys. Chem. 75 (2006) 1977.
[28] N. Saito, et al., J. Electron Spectrosc. Relat. Phenom. 144–147 (2005) 103.
[29] K. Ueda, J.H.D. Ealnd, J. Phys. B: At. Mol. Opt. Phys. 38 (2005) S839.
[30] Y. Morishita, et al., J. Electron Spectrosc. Relat. Phenom. 144–147 (2005) 255.
[31] G.C. King, et al., J. Phys. B: At. Mol. Opt. Phys. 10 (1977) 2479.
[32] K. Hosaka, et al., J. Phys. B: At. Mol. Opt. Phys. 37 (2004) L49.
[33] R.R. Lucchese, et al., Phys. Rev. A 65 (2002) 020702.
[34] R. Santra, et al., Phys. Rev. Lett. 85 (2000) 4490.
[35] V. Averbukh, I.B. Müller, L.S. Cederbaum, Phys. Rev. Lett. 93 (2004) 263002.
[36] V. Averbukh, L.S. Cederbaum, Phys. Rev. Lett. 96 (2006) 053401.
[37] R. Santra, L.S. Cederbaum, Phys. Rev. Lett. 90 (2003) 153401; R. Santra, L.S. Cederbaum, Phys. Rev. Lett. 94 (2005) 199901E.
[38] T. González-Lezana, et al., J. Chem. Phys. 110 (1999) 9000.
[39] http://physics.nist.gov/PhysRefData/ASD/levels_form.html.